Journal of
Materials Chemistry B

PAPER

View Article Online
View Journal | View Issue

Cite this: J. Mater. Chem. B, 2016, 4, 5385

Antibacterial bioadhesive layer-by-layer coatings for orthopedic applications†

A. L. Carvalho,‡[ab] A. C. Vale,‡[ab] M. P. Sousa,[ab] A. M. Barbosa,[bc] E. Torrado,[bc] J. F. Mano[ab] and N. M. Alves*[ab]

Received 5th April 2016,
Accepted 15th July 2016

DOI: 10.1039/c6tb00841k

www.rsc.org/MaterialsB

In this study, thin LbL films were produced by combining the adhesive properties of the hyaluronic acid–dopamine conjugate with the bioactivity and bactericidal properties of silver doped bioactive glass nanoparticles. The build-up of these films was investigated by quartz crystal microbalance with dissipation monitoring. LbL coatings were then constructed on a glass substrate for further characterization. We found that these antimicrobial bioinspired films display enhanced adhesive strength. *In vitro* bioactivity tests were performed by immersing them in simulated body fluid solution for 14 days where the constructed films promoted the formation of a bone-like apatite layer. From microbiological assays, it was found that coatings containing silver doped nanoparticles exhibited a remarkable antibacterial effect against *Staphylococcus aureus* and *Escherichia coli* cultures. Finally, *in vitro* cellular behavior tests showed enhanced cell adhesion, proliferation and viability for these antibacterial bioadhesive films. Therefore, the constructed thin films showed promising properties and evidenced great potential to be used as coatings for orthopedic implants.

Introduction

It is well known that one major complication of bone reconstruction is the development of bacterial infections. Ideally, the implant should have the ability to regenerate bone tissue and to treat the infection by delivering an antibacterial agent in a controlled and continuous manner.[1] The development of an adhesive substrate that enhances the adhesion to the tissue and cell attachment and proliferation, and simultaneously inhibits the development of bacterial infections would constitute a substantial boost for biomedical applications.

Recently, adhesives found in nature, such as the ones inspired by marine mussels, have attracted widespread interest and are now exploited by various synthetic approaches, due to their outstanding adhesive properties under the harsh conditions of the sea. The liquid protein adhesives secreted by these organisms rapidly harden to form a solid adhesive plaque capable of mediating firm attachment to a variety of wet surfaces. These mussel adhesive proteins (MAPs) contain high concentrations of L-3,4-dihydroxyphenylalanine (DOPA).[2] A defining feature of DOPA and its analogue dopamine is the *ortho*-dihydroxyphenyl (catechol) functional group, capable of creating strong bonds in aqueous environments with numerous inorganic or organic surfaces.[3–10]

Many techniques have been applied in the production of functional coatings. One of the most used and advantageous techniques is the layer-by-layer (LbL) technique, due to its simplicity. LbL is a versatile methodology that enables the construction of coated surfaces through multiple deposition steps with an ability to control the build-up of complex geometries at the nanometer length scale. This constitutes a great advantage in comparison to the other thin film techniques.[11,12]

In the present work, multilayer coatings were produced by LbL using chitosan (CHT), dopamine modified hyaluronic acid (HA–DN) and silver doped bioactive glass nanoparticles (AgBG). These new multifunctional mussel inspired LbL films were developed in order to combine the favourable cell response of the biomaterials and also the adhesion properties found in marine mussels, the bioactivity of bioglass nanoparticles and the antimicrobial properties of silver by a simple film production method. As far as we know, it is the first time that such a combination of properties can be found in a thin coating.

In fact, chitosan and hyaluronic acid have been used in many biomedical applications due to their properties. Chitosan is a polysaccharide composed of glucosamine and *N*-acetyl glucosamine linked by a β-1-4-glycosidic linkage. Due to the

[a] 3B's Research Group – Biomaterials, Biodegradables and Biomimetics, University of Minho, Headquarters of the European Institute of Excellence on Tissue Engineering and Regenerative Medicine, AvePark, 4805-017 Barco, Guimarães, Portugal. E-mail: nalves@dep.uminho.pt
[b] ICVS/3B's PT Associate Laboratory, Guimarães, Portugal
[c] Life and Health Sciences Research Institute (ICVS), School of Health Sciences, University of Minho, Braga, Portugal

† Electronic supplementary information (ESI) available. See DOI: 10.1039/c6tb00841k

‡ Authors contributed equally (co-first authors).

primary amines present in its structure, it is a positively charged polyelectrolyte in acidic medium, with a $pK_a \approx 6.24$.[12–17] CHT is a biopolymer, which is biocompatible and can be degraded by enzymes in the human body, the degradation products being nontoxic.[17] Hyaluronic acid is a negatively charged polysaccharide that can be found in tissues and body fluids of vertebrates and also in some bacteria and plays an important role in initiating the biological reactions, such as early- and long-range engagement between cells and substrates.[18,19] On the other hand, silver is one of the most interesting antibacterial materials due to the excellent broad-spectrum antimicrobial properties provided by its ions, which are particularly significant in preventing polymicrobial colonization that causes the common infections developed in biomedical applications for wound repair.[17,20,21] The antibacterial effect of silver ions is well documented.[22] In particular, it was found that silver ions kill microorganisms instantly by blocking their respiratory enzyme systems, while having no negative effect on human cells.[20,23] Bioactive glass nanoparticles containing silver have been produced by different techniques (sol–gel, melting, and ion exchange) and, as antibacterial agents, these doped nanoparticles have attracted significant attention in recent years,[23–25] since the incorporation of silver ions into the glass matrix allows the controlled delivery of these antibacterial agents at the site of the bone infection.[1]

From these previous findings, it is expected that the produced films could be used in biomedical applications, for example, as coatings for orthopedic implants, in order to improve both cell response and osteoconductivity and also to prevent bacterial infections. Firstly, silver doped bioactive glass nanoparticles (AgBG) were prepared by a sol–gel method. Then, the LbL build-up of chitosan (CHT), dopamine modified hyaluronic acid (HA–DN) and AgBG was investigated *in situ* using quartz crystal microbalance with dissipation monitoring (QCM-D). The adhesive strength of the LbL coatings produced on glass substrates was analyzed by lap shear tests. After immersion of these coatings in simulated body fluid solution (SBF) for 7 days and 14 days, the bioactivity was investigated by scanning electron microscopy coupled with energy dispersive X-ray spectroscopy (SEM-EDS), Fourier transform infrared spectroscopy (FTIR) and X-ray diffraction (XRD). The antibacterial susceptibility of the constructed multilayer coatings was evaluated by disk diffusion tests performed with Gram-negative (*Escherichia coli*) and Gram-positive (*Staphylococcus aureus*) bacteria. Finally, the *in vitro* biocompatibility of these coatings was also tested by direct contact tests with L929 cells.

Experimental

Materials

Medium molecular weight chitosan (CHT, an *N*-deacetylation degree of 80% and a molecular weight of 770 kDa), hyaluronic acid sodium salt from *Streptococcus equi* (HA, molecular weight of 595 kDa), dopamine hydrochloride (DN), *N*-(3-dimethylaminopropyl)-*N*′-ethylcarbodiimide hydrochloride (EDC, purum, ≥98.0% (AT)), dialysis tubing, benzoylated avg. flat width 32 mm (1.27 inch), ammonium phosphate dibasic, calcium nitrate tetrahydrate 99%, ethanol absolute, ammonia water (ammonium hydrogen phosphate 98%, maximum of 33% NH_3), sodium chloride (NaCl), sodium of hydrogen carbonate ($NaHCO_3$), magnesium chloride hexahydrate ($MgCl_2{\cdot}6H_2O$), calcium chloride ($CaCl_2$), sodium sulfate (Na_2SO_4), tris(hydroxymethyl)–aminomethane (Tris buffer, $(CH_2OH)_3CNH_2$), hydrochloric acid (HCl) and silver nitrate ($AgNO_3$) were acquired from Sigma-Aldrich (St. Louis, MO, USA). Tetraethyl orthosilicate (TEOS, 99.90%) was purchased from Merck KGaA (Darmstadt, Germany). Nitric acid monohydrate (69%), potassium chloride (KCl), acetone and 2-propanol were obtained from VWR International (UK). Sodium hydroxide (NaOH) was purchased from Fisher Chemical (Fisher Scientific UK, Leics, UK) and hydrogen peroxide 30% (w/v) was obtained from Panreac AppliChem (Darmstadt, Deutschland). Sodium of hydrogen carbonate ($NaHCO_3$), dipotassium hydrogen phosphate trihydrate ($K_2HPO_4{\cdot}3H_2O$) and calcium chloride ($CaCl_2$) were purchased from Merck (Merck Sharp & Dohme Corp., Kenilworth, NJ, USA). Standard gold QCM-D sensor crystals (QSX 301 Gold, Au 100 nm, 14 mm diameter) were purchased from Q-Sense (BiolinScientific, Stockholm, Sweden). For microbial tests, Mueller-Hinton agar (MHA) medium was purchased from ThermoScientific (Thebarton, SA, Australia) and standardized cultures of *Staphylococcus aureus* (ATCC 29213TM) and *Escherichia coli* (ATCC 25922TM) with 1.5×10^8 CFU were purchased from the American Type Culture Collection (Manassas, VA, USA). For the cellular behavior assays, the mouse fibroblast cell line L929 was obtained from European Collection of cell cultures (ECACC, UK). Dulbecco's modified minimum essential medium (D-MEM), fetal bovine serum (FBS), phalloidin–tetramethylrhodamine B isothiocyanate and DAPI (4′,6-diamidino-2-phenylindole) were purchased from Sigma-Aldrich (St. Louis, MO, USA). MTS (3-(4,5-dimethylthiazol-2-yl)-5-(3-carboxymethoxyphenyl)-2-(4-sulfophenyl)-2*H*-tetrazolium) was obtained from VWR International (UK).

Hyaluronic acid–dopamine conjugate synthesis

Hyaluronic acid sodium salt from *Streptococcus equi* was modified with the catechol groups of dopamine hydrochloride, called the hyaluronic acid–dopamine conjugate (HA–DN), following the experimental procedure for the synthesis of dopamine-conjugated HA proposed by Lee and co-workers,[5] but with some modifications. One tablet of phosphate buffered saline was dissolved in osmotized water (200 mL). HA (1 g) was dissolved in 0.01 M PBS solution (100 mL) and the pH was adjusted to 5.5 using 0.5 M hydrochloric acid (HCl) or 0.5 M sodium hydroxide (NaOH) aqueous solutions. The solution was purged with nitrogen for 1 h to limit the oxygen interaction with the solution. HA–DN conjugates were synthesized using 1-ethyl-3-(3-dimethylaminopropyl)carbodiimide hydrochloride (EDC) as an activation agent of the carboxyl groups on HA chains. EDC (338 mg) and DN (474 mg) were added to the above hyaluronic acid solution with an acidic pH of 5.5, and this mixture was maintained under slow stirring for 2 hours, or until the complete dissolution of these distinct reagents. Finally, the unreacted chemicals and urea byproducts were removed by

dialysis using osmotized water for a week, and then the conjugate was lyophilized for 4 days.

The reaction was performed at 4 °C and protected from light, in order to avoid the oxidation of DN, since dopamine is sensitive to air and light. In this sense, the produced conjugate was stored at −20 °C and protected from light. The HA–DN conjugate synthesized using the described procedure presents a substitution degree of 11%.[11]

Silver doped bioactive glass nanoparticle production

Silver doped bioactive glass nanoparticles were produced following the protocol for the production of ternary glass nanoparticles with some modifications, based on the procedure proposed by El-Kady *et al.*[1] These doped nanoparticles were also prepared by a sol–gel methodology, containing the following formulation: [SiO_2–CaO–P_2O_5–Ag_2O (mol%): 56–30–4–10].

Firstly, at room temperature, osmotized water (13.9 mL) was added to TEOS (20.8552 mL) and, then, added together with ethanol absolute (50 mL). The pH value of this solution was adjusted to 2 with 2 M nitric acid solution and the reaction mixture was kept stirring for 60 min to produce solution A. Then, for preparation of solution B, calcium nitrate tetrahydrate (11.9045 g), ammonium phosphate dibasic (0.8876 g) and silver nitrate (2.8544 g) were added to osmotized water (1500 mL) and the pH value was adjusted to 11.5 with ammonium hydroxide solution. The reaction mixture was kept under stirring for 60 min. Under smooth stirring, solution A was slowly added to solution B drop-by-drop. During this step, the pH value of solution B was maintained at 11.5 using ammonia hydroxide solution. Then, the final solution was kept under stirring for 48 h. Finally, after drying the gel at 130 °C for 24 h in a drying oven, it was treated at 600 °C for 4 hours, to eliminate organic residues and to obtain the AgBG nanoparticles.

QCM-D analysis of the multifunctional LbL film construction

The step-by-step build-up of these multilayer films was analyzed *in situ* by quartz crystal microbalance with dissipation monitoring, QCM-D (Q-Sense, E4 system, Sweden), in order to find the optimal conditions for an accurate LbL assembly. The combination of normalized resonant frequency ($\Delta f/\upsilon$) and energy dissipation (ΔD) measurements available with this technique gives information about the adsorbed amount (*via* $\Delta f/\upsilon$) and the variation of the viscoelastic properties (*via* ΔD) of the constructed film in real time. If a rigid mass is adsorbed onto the surface of the piezoelectric crystal there will be a decrease in the oscillation frequency. For viscoelastic materials, the adsorbed mass does not fully couple to the oscillation of the crystal and dampens the oscillation.

Medium molecular weight chitosan was used as the polycation, while HA–DN and AgBG acted as the polyanion. Fresh polyelectrolyte solutions were prepared by dissolution of HA–DN and CHT in 0.15 M NaCl solution to yield a final concentration of 0.5 mg mL^{-1}, while the final concentration of AgBG suspension was 2.5 mg mL^{-1}. Due to the solubility of CHT in acidic solutions, the CHT solution was prepared with 1% (v/v) acetic acid. On the other hand, before the QCM experiments, the AgBG suspension was dispersed in an ultrasonic water bath (DT100H SONOREX, Bandelin electronic GmbH & Co. KG, Berlin, Deutschland) for 15 min to avoid the aggregation and precipitation of nanoparticles.

Optically polished gold deposited quartz crystals (14 mm diameter, QSX301 Gold, Q-Sense) were used, which were excited at 5 MHz, as well as at 15, 25, 35, 45 and 55 MHz corresponding to the 3rd, 5th, 7th, 9th and 11th overtones. The crystals were previously cleaned with a 5 : 1 : 1 mixture of osmotized water, ammonium hydroxide solution and hydrogen peroxide 30% (w/v) overnight and then, by sequential sonication for 3 minutes in acetone, ethanol absolute, 2-propanol, and osmotized water and, finally, dried with flowing nitrogen gas avoiding contamination prior to use. In order to ensure that QCM-D crystals are perfectly clean and, therefore, they show a null frequency, all the experiments were started with the injection of 0.15 M sodium chloride solution as a baseline. Then, the CHT/HA–DN solutions were injected into the QCM-D chambers for 10 minutes, while AgBG suspension was injected into the cell for 20 minutes at a flow rate of 50 μL min^{-1}. A rinsing step of 5 minutes with the solvent (0.15 M NaCl) was included between the adsorptions of each polyelectrolyte. The multilayer systems with 12 layers were assembled at 25 °C and pH 5.5 that was adjusted with HCl or NaOH solutions. Control films, containing hyaluronic acid unmodified, were also prepared for comparison. During the entire process $\Delta f/\upsilon$ and ΔD shifts were continuously recorded as a function of time. The QCM-D response of a viscoelastic film, such as the films produced in this work, can be modeled using a Voigt based model[26] defined as a spring and dashpot in parallel under no slip conditions (eqn (S1) and (S2) in the ESI†).

From these QCM-D experiments, the thickness of the constructed LbL films was estimated using the Voigt viscoelastic model implemented in the QTools software (Q-Sense), assuming a fluid density of 1000 kg m^3, a layer density of 1200 kg m^3 and a fluid viscosity of 1 mPa s.

Adhesion tests

The adhesion strength of the thin films constructed onto the glass substrate was evaluated through lap-shear stress tests performed using a universal electromechanical testing machine (Instron model 5540, USA) with a load-cell of 1 kN, following the ASTM D1002 standard.

For construction of the multilayer films onto the glass substrate, fresh polyelectrolyte solutions were prepared with 0.15 M NaCl solution and pH 5.5, at room temperature: 0.5 mg mL^{-1} CHT solution with 1% (v/v) acetic acid; 0.5 mg mL^{-1} HA/HA–DN solution; and 2.5 mg mL^{-1} AgBG suspension. Distinct films were produced: the multifunctional films containing the hyaluronic acid–dopamine conjugate: condition 1 [CHT/HA–DN/CHT/AgBG]$_5$ + CHT/HA–DN; condition 2: [CHT/HA–DN/CHT/AgBG]$_5$; and the control films without dopamine: control 1: [CHT/HA/CHT/AgBG]$_5$ + CHT/HA; and control 2: [CHT/HA/CHT/AgBG]$_5$.

Both multifunctional and control films were also prepared either ending with a HA–DN/HA layer or with a AgBG layer, as shown in Fig. 1. The aim of using different configurations was to study the influence of the end layer on their adhesive,

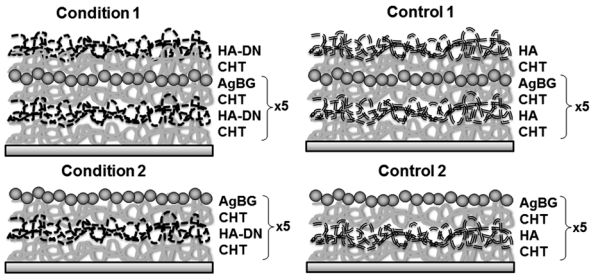

Fig. 1 Schematic of the constructed multilayer film configurations. Condition 1: $[CHT/HA–DN/CHT/AgBG]_5$ + CHT/HA–DN; condition 2: $[CHT/HA–DN/CHT/AgBG]_5$; control 1: $[CHT/HA/CHT/AgBG]_5$ + CHT/HA; and control 2: $[CHT/HA/CHT/AgBG]_5$.

bioactivity and bactericidal properties, depending on whether they end with nanoparticles or with the hyaluronic acid–dopamine conjugate.

Glass plaques with 3 mm of thickness were alternately dipped in the polyelectrolyte solutions, in order to produce films with 10 or 11 layers, depending on their film configuration. A rinsing step with 0.15 M NaCl solution was included between the adsorptions of each polyelectrolyte.

After the LbL construction, a pair of plates was put in contact with an overlapped area of 10 × 20 mm^2 and maintained at 37 °C overnight. Then, the bonded glass slides were placed on the testing machine and they were stressed, at a speed of 5 mm min^{-1}, until their detachment and they were pulled apart. All adhesion experiments were conducted at room temperature (25 °C). The adhesion strength was determined from the maximum of the force–deformation experimental curve, and the mean and standard deviation values were determined using the results from five tested samples.

In vitro bioactivity studies

Standard *in vitro* bioactivity studies were conducted by immersion of the multilayer films in simulated body fluid (SBF) solution. The SBF solution was prepared according to the Kokubo and Takadama protocol[27] by the dissolution of sodium chloride, sodium hydrogen carbonate, potassium chloride, dipotassium hydrogen phosphate trihydrate, magnesium chloride hexahydrate, calcium chloride and sodium sulfate in osmotized water. The pH was adjusted to 7.4 using tris(hydroxymethyl)aminomethane buffer and hydrochloric acid.

SBF is usually used because it simulates the concentration of ionic species present in human blood plasma. Each coated glass coverslip with 10 × 10 mm^2 was immersed, for 7 and 14 days, in 25 mL of SBF solutions at 37 °C. After being removed from SBF solution, the coverslips were cleaned with ultra-pure water and dried at room temperature.

The formation of apatite on the surface of the films was characterized by their surface analysis, using distinct techniques such as scanning electron microscopy (JSM-6010 LV, JEOL, Japan) coupled with energy dispersive X-ray spectroscopy (INCAx-Act, PentaFET Precision, Oxford Instruments), Fourier Transform infrared spectroscopy (Perkin-Elmer 1600 series equipment, USA), and X-ray diffraction (Bruker AXS D8 Discover, USA).

Microbiological analysis

To test the antimicrobial properties of LbL films, the disk diffusion methodology was performed. Briefly, the LbL films $[CHT/HA–DN]_{10}$, $[CHT/HA–DN/CHT/BG]_5$, $[CHT/HA–DN/CHT/AgBG]_5$, $[CHT/HA–DN/CHT/BG]_5$ + [CHT/HA–DN] and $[CHT/HA–DN/CHT/AgBG]_5$ + [CHT/HA–DN] were produced in 0.5 cm glass squares. Glass squares were then placed on top of a Mueller-Hinton agar plate inoculated with 1.5 × 10^8 CFU of a standardized culture of *Staphylococcus aureus* or *Escherichia coli* (OD600 of approximately 0.1) and incubated for 16 h at 37 °C. The formation of an inhibition zone surrounding the LbL coated glass squares was used as an indicator of antibacterial activity.

Cellular behavior

The mouse fibroblast cell line L929 was chosen to test the *in vitro* cellular behavior with the developed coatings. This cell line was obtained from European Collection of cell cultures (ECACC, UK). Direct contact tests were performed. Prior to cell seeding, the samples were sterilized/disinfected by immersion in 70% (v/v) ethanol for 2 hours and then they were washed twice with sterile phosphate buffered saline. The cells were cultured with Dulbecco's modified minimum essential medium supplemented with 10% fetal bovine serum and 1% antibiotic, incubated at 37 °C in a humidified air atmosphere of 5% CO_2 and placed to grow until confluence modifying the culture medium each 2 days. When confluence reached 90%, the cells were seeded onto the samples (n = 3) at a density of 1 × 10^4 cells per sample and incubated at 37 °C. After 4 hours, supplemented DMEM was added to each well to nourish the adhered cells.

MTS assay. After specific time points (1, 3 and 7 days), a MTS (3-(4,5-dimethylthiazol-2-yl)-5-(3-carboxymethoxyphenyl)-2-(4-sulfophenyl)-2*H*-tetrazolium) assay was performed in order to evaluate the cytotoxicity of the coating and compare the relative cellular viability between each condition and a positive control, the tissue culture polystyrene (TCPS). The samples were immersed with a solution composed of a 1 : 5 ratio of MTS reagent and DMEM culture medium without phenol red or FBS, and then were incubated for a period of 3 hours at 37 °C. All cytotoxicity tests were conducted by using 3 replicates. Finally, the optical density (OD) was read at 490 nm on a multiwell microplate reader (Synergy HT, Bio-Tek Instruments).

Live-dead assay. After specific time points, 3 days and 7 days, the medium was aspirated from each well and the material was washed with PBS. The modified substrates were incubated at 37 °C, with ethidium homodimer 1 (4 μM) and calcein AM (2 μM), both in PBS, for 15 minutes. Then, the samples were quickly observed through an inverted fluorescence microscope (Transmitted and Reflected Light Microscope with Apotome 2, Zeiss, Germany) and the images were acquired and processed using the AxioVision software version: Zeiss 2012 (Zeiss, Germany).

Phalloidin/DAPI observation. To obtain fluorescence images, the samples were firstly fixed, at each time point, with a solution

of 10% of formalin for 30 minutes; then these samples were washed with PBS. The samples were then labeled with fluorescent stains: phalloidin–tetramethylrhodamine B isothiocyanate, which binds to actin filaments (staining the cytoskeleton of the cells in red), was incubated with samples at 1 : 200 in PBS for 45 min and DAPI (4′,6-diamidino-2-phenylindole), which binds specifically to DNA regions (staining cell nuclei in blue), was added at 1 : 1000 in PBS for 15 min. This procedure was always done protecting from light, and in the end the samples were washed twice with PBS and left overnight. The resulting fluorescence images were taken from these samples, in the dark, using again the fluorescence microscope (Transmitted and Reflected Light Microscope with Apotome 2, Zeiss, Germany) and the images were acquired and processed using the AxioVision software version: Zeiss 2012 (Zeiss, Germany).

Statistical analysis

All experiments were carried out at least in triplicate and their results were presented as a mean ± standard deviation (SD). Statistical significance between groups was determined by one-way ANOVA with Tukey's *post test* using Graph Pad Prism version 5.0 (GraphPad software, San Diego, CA). Only statistical differences were represented and they were set to $p < 0.01$(**) and $p < 0.0001$(***).

Results and discussion

Build-up of multilayer antibacterial films

In the present work the construction of the multifunctional films was monitored *in situ* by QCM-D. Fig. 2 summarizes the main results obtained for the build-up of the film with configuration $[CHT/HA–DN/CHT/AgBG]_6$ and also for its respective control $[CHT/HA/CHT/AgBG]_6$. Fig. 2A and B show the mean value of the normalized frequency ($\Delta f/\upsilon$) and dissipation (ΔD) as a function of each deposited bilayer for the 7th overtone and based on three QCM-D experiments. The normalized frequency is related to mass uptake, while the energy dissipation allows us to get information about the viscoelastic properties.[28] As Fig. 2A and B evidence, after each polyelectrolyte deposition, there is a decrease of $\Delta f/\upsilon$. On the other hand, the increase of ΔD proves that these films are not rigid, since they dissipate energy during their construction. So, the constructed films showed a viscoelastic behavior, which is typically evidenced by polymeric systems. The cumulative thickness evolution is also provided in Fig. 2C and the final thickness obtained for the control film is approximately 87 nm, which is lower than for the antimicrobial bioinspired film (184 nm).

Comparing these results with a similar LbL construction without bioactive glass nanoparticles previously obtained by our group[11] for 10 layers, it can be seen that the produced films ($[CHT/HA–DN/CHT/AgBG]_5$ + CHT/HA–DN, thickness ~40 nm; $[CHT/HA/CHT/AgBG]_5$ + CHT/HA, thickness ~53 nm) have a lower thickness than those obtained without bioactive nanoparticles ($[CHT/HA–DN]_5$, thickness ~75 nm),[11] which probably indicates that the addition of inorganic surfaces turns the films more compact. On the other hand, these QCM-D experiments show a substantial difference in the normalized frequency values of the control film when compared with the antimicrobial bioinspired film ($[CHT/HA–DN/CHT/AgBG]_6$), suggesting that in contrast to our previous findings,[11,29] the control film is thinner, more rigid and less water-rich. Nevertheless, the most important finding shown is that depositions were stable, and hence these antimicrobial bioinspired films could be successfully assembled using the LbL technique.

Adhesive strength of distinct antibacterial films

The adhesive strength of the multilayer coatings to a glass substrate was evaluated using a universal mechanical testing machine (Instron model 5540, USA). Pairs of samples with different LbL coating configurations were bonded and then placed on the electromechanical testing machine, at room temperature. The samples were stressed until enough force was applied to trigger their detachment and pull them apart. Then, the adhesive strength was determined from the maximum of the force–deformation curve obtained. Fig. 3 presents the mean values of adhesive strength obtained from five lap shear tests performed for each distinct LbL film configuration illustrated in Fig. 1. These mechanical tests show that the antibacterial thin films present a higher adhesive strength when compared with their controls (without HA–DN). In fact, our group[11] has already shown that the films containing hyaluronic acid modified with dopamine evidence enhanced adhesive properties, where an

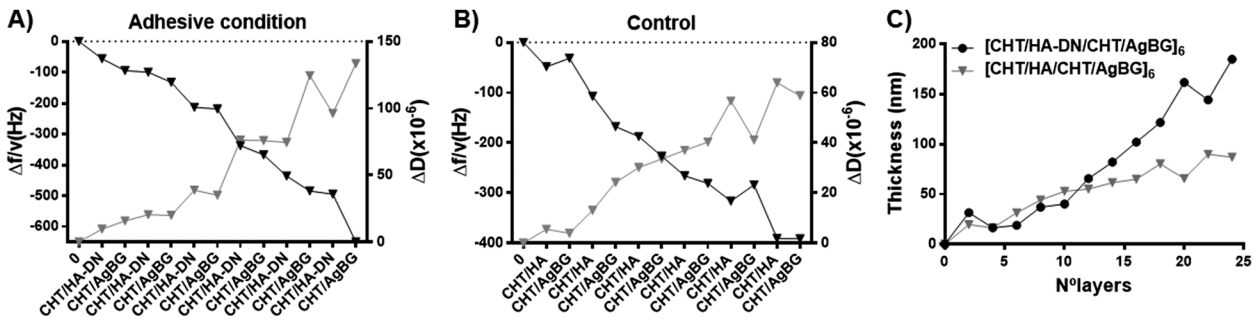

Fig. 2 Build-up assemblies on quartz crystal microbalance with dissipation (QCM-D) for (A) antimicrobial bioadhesive coating $[CHT/HA–DN/CHT/AgBG]_6$ and (B) respective control, $[CHT/HA/CHT/AgBG]_6$. (C) Thickness evolution of $[CHT/HA–DN/CHT/AgBG]_6$ and $[CHT/HA/CHT/AgBG]_6$ films as a function of the number of deposited layers.

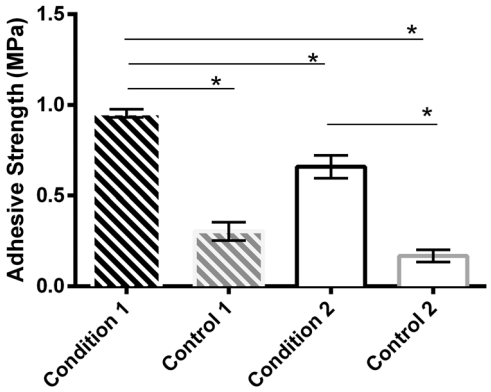

Fig. 3 Adhesive strength of four LbL film conditions. Condition 1: [CHT/HA–DN/CHT/AgBG]$_5$ + [CHT/HA–DN], control 1: [CHT/HA/CHT/AgBG]$_5$ + [CHT/HA], condition 2: [CHT/HA–DN/CHT/AgBG]$_5$, and control 2: [CHT/HA/CHT/AgBG]$_5$. Statistically significant adhesive strength as compared with distinct conditions is shown (*$p < 0.05$), $n = 5$; mean ± standard deviation condition shown.

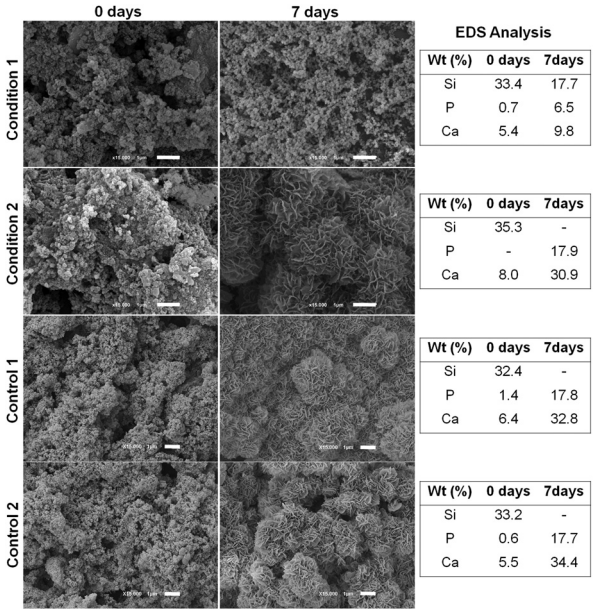

Fig. 4 *In vitro* bioactivity studies. Representative SEM images and respective quantitative EDS analysis of four LbL film configurations (see Fig. 1), before and after SBF immersion for 7 days. The scale bar represents 1 μm.

adhesive strength of 2.32 MPa was found for the film [CHT/HA–DN]$_5$ and 0.75 MPa for [CHT/HA]$_5$.[11] On the other hand, in another previous work,[29] we already found improved adhesive properties for LbL films with dopamine and ternary bioactive nanoparticles in their structure, but it should be mentioned that the adhesive strength obtained in this work is somewhat lower than those in previous results, probably due to some oxidative effect of the silver ions released from the incorporated nanoparticles. In fact, the reduction of the adhesive properties, due to the presence of silver, was already reported by Perelshtein *et al.*[30]

In vitro bioactivity tests

The *in vitro* bioactivity of the constructed LbL films was studied through the detection of the apatite layer formation on the film surface after their immersion in SBF. In this way, their surface analysis was investigated using scanning electron microscopy (JSM-6010 LV, JEOL, Japan) coupled with energy dispersive X-ray spectroscopy (INCAx-Act, PentaFET Precision, Oxford Instruments).

Fig. 4 shows the SEM micrographs and the respective EDS quantification, revealing the elemental composition of the film surface from different LbL configurations, which confirms the development of the apatite precipitation during the *in vitro* study.

After SBF immersion (7 days), nucleation and growth of particles occurred on the substrate surface and mineral agglomerates could be observed; the apatite formation can also be seen around the film. In addition, after 7 days, the EDS quantification of both conditions shows a decrease of Si concentration and an increase of Ca and P concentrations,[31] as a consequence of the nanoparticle dissolution. With these results, it is possible to confirm the bioactive behavior of all LbL configurations tested, which promote the development of the typical cauliflower morphology of apatite crystals.

Fig. S1A (ESI†) presents the FTIR spectra of the film surface, before and after 14 days of SBF immersion. Before SBF immersion, the typical wavenumber of silicate absorption was found to be 1085 cm^{-1} (asymmetric stretching mode) and 800 cm^{-1} (symmetric stretching vibration). Fig. S1B (ESI†) presents the XRD characterization for four LbL film configurations, before (0 day) and after immersion in SBF solution (14 days). As expected, the XRD spectrum at 0 days shows an amorphous profile, which can be related to the glass substrate used. After 14 days of immersion, some bands tend to disappear due to the decrease of Si percentage after SBF immersion, but all spectra reveal the typical crystalline peaks of hydroxyapatite at $2\theta = 15$ to 35° and the presence of the band of the P–O bending vibration clearly evidences the growth of hydroxyapatite due to the crystalline calcium phosphate phase (600 to 550 cm^{-1}).[32] Since the XRD patterns have the typical hydroxyapatite diffractogram, as previously reported in other works,[31,32] it is possible to conclude that the produced films present bioactive character, which is of utmost importance for its application as a coating for orthopedic implants.

Microbiological analysis

The antimicrobial properties of the produced films were investigated using the disk diffusion methodology. Fig. 5 shows that only films containing the AgBG layer have antibacterial properties against *S. aureus* and *E. coli*, as demonstrated by the inhibitory zone formed around the coated glass squares. These data show that the addition of the AgBG layer to LbL coatings adds important antimicrobial properties to these coatings. Indeed, in contrast to the LbL coatings containing ternary nanoparticles, there is an inhibition of bacterial growth around coatings containing AgBG. Furthermore, the addition of an HA–DN layer after the addition of the AgBG layer does not impact the antimicrobial properties of the LbL coatings. The relatively small inhibitory zone formed surrounding the coated glass squares is likely a result of the reduced release of Ag from the glass substrate, as previously shown.[1]

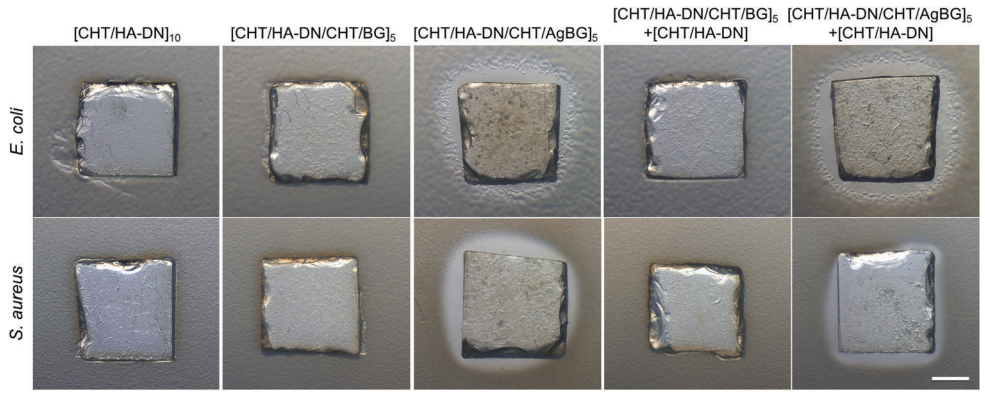

Fig. 5 Images of LbL coatings 16 h after being placed on top of a Mueller-Hinton agar plate with *E. coli* and *S. aureus* (1.5×10^8 CFU) incubated at 37 °C. The antimicrobial behaviour of the LbL coatings is demonstrated by the formation of an inhibitory zone surrounding the $[CHT/HA–DN/CHT/AgBG]_5$ and $[CHT/HA–DN/CHT/AgBG]_5$ + [CHT/HA–DN] coatings. The scale bar represents 2000 μm.

Chatzistavrou *et al.*[33] have previously shown that this type of nanoparticle maintains bactericidal properties, even for composites with a lower concentration of silver. These effects were attributed to the silver ions released during the dissolution of nanoparticles. Bellantone *et al.*[20] also corroborated these data and showed that the antimicrobial properties of AgBG on *S. aureus* and *E. coli* were attributed to the silver ions leaching out of the glass matrix. The released ions bind to multiple bacterial structures, including the cell wall, plasma membrane, DNA and proteins creating structural abnormalities and preventing bacterial replication.[34] Therefore, the potential for bacteria to develop resistance to silver is lower than to antibiotics. With *Staphylococci* comprising up to two-thirds of all pathogenic infections associated with orthopedic implants,[35] the incorporation of these AgBG in orthopedic devices has great potential to reduce the incidence of implant associated infections.

Cellular behavior

Finally, a L929 fibroblast line was used to evaluate the cellular behavior of the developed coatings: this choice was made because L929 is a standard cell line typically used in the biomedical field.

Firstly, cellular viability was evaluated by performing a MTS assay, where the metabolic activity of the cells can be achieved through the chemical reduction of the MTS compound to formazan. Fig. 6A presents the results obtained from MTS assay for 1, 3 and 7 days, and essentially, the highest absorbance value corresponds to higher metabolic cellular activity, which indicates a higher number of cells. Five conditions were considered: $[CHT/HA/CHT/AgBG]_5$ + [CHT/HA]; $[CHT/HA/CHT/AgBG]_5$; $[CHT/HA–DN/CHT/AgBG]_5$; $[CHT/HA–DN/CHT/AgBG]_5$ + [CHT/HA–DN], and a positive control (TCPS), where cells were supposed to have a great proliferation. Cellular proliferation was relatively evaluated through MTS assay: in the first 3 days differences between the different conditions and also in the cytotoxicity of the coatings were not observed. A live–dead assay was also performed and, in Fig. 6B, it is possible to observe live–dead images of the different conditions at different timepoints and as we can notice for every case, there was a minimal percentage of dead cells (in red), discarding the cytotoxic effects of the different coatings. Note that all images are representative for all conditions. At day 7, differences between the coatings were clearly noted through the live-dead assay. Five representative areas of each condition were chosen to estimate the live–dead ratio and from these results, at day 7, for the condition ending with CHT/HA–DN we obtained a live–dead ratio of 22.9 ± 3.01, showing higher viability. This ratio decreased for the conditions ending with AgBG: 8.4 ± 2.13 for the multilayer containing entrapped DN and 10.9 ± 2.42 for the other. When compared to the others, the condition ending with CHT/HA presents a lower value of the live-dead ratio 3.5 ± 0.99, in accord with what we obtained for MTS results. Here, the relative cellular viability was significantly higher for the coating that ends with HA–DN, compared with the control without dopamine and even with the one that has HA–DN and AgBG as end layers.

The MTS assay clearly suggested that the last layer has a great influence on the cellular response and, in particular, the presence of the catechol groups of dopamine is critical for better cell viability and proliferation. In the last few years other works have reported better cellular performance substrates modified with dopamine.[11,19,36,37] At day 7, comparing the samples with AgBG, in the last layer and the sample ending with CHT/HA, it was clear that cell viability and metabolic activity were higher for the first ones. It can be related to the rate of release of AgBG; the coatings with the end layers composed of AgBG showed a faster release than the one ending with CHT/HA where AgBG was more strongly entrapped inside the multilayer coating and took more time to be released. The literature[38,39] already reported the effect of AgBG on cellular behavior and when at higher concentration, these particles can decrease the cellular viability and proliferation. Therefore, we think that the cellular viability and compatibility were significantly lower for the sample ending with CHT/HA because of the slow release of these nanoparticles.

Overall, when culturing the cells for 3 days, no evident differences were observed amongst the different conditions but interestingly, after this time we noted an obvious increase of cell proliferation and viability. This can be explained through the release of silver from the coating: Wang *et al.*[37] reported

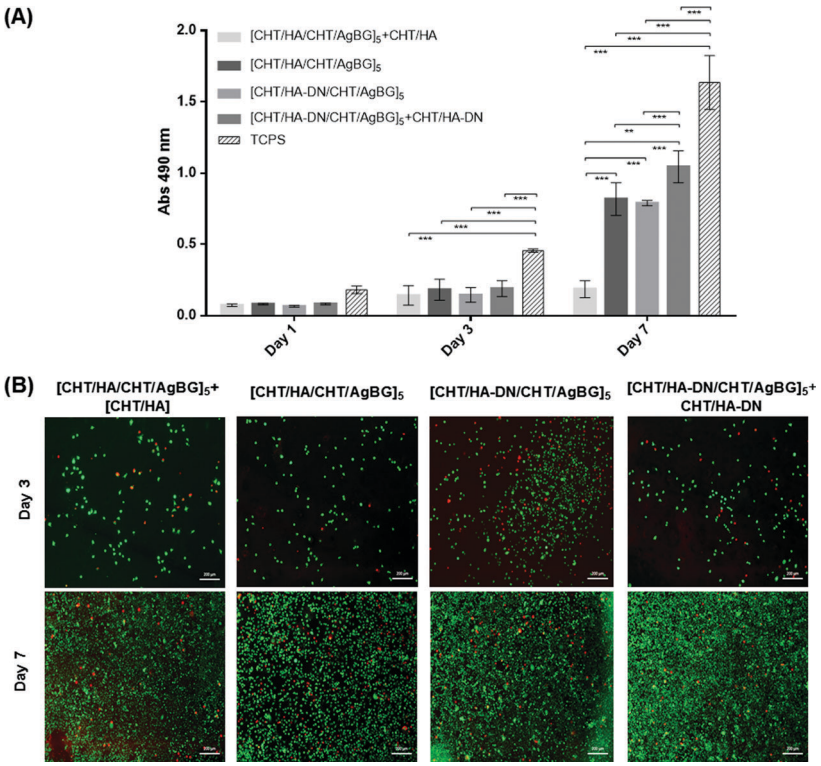

Fig. 6 L929 viability results obtained through (A) MTS assay for 1, 3 and 7 days, where absorbance was read at 490 nm. Statistically significant differences between distinct substrates by each time point are marked with ** and ***, which represents $p < 0.01$ and $p < 0.001$, respectively. Regarding statistical differences related to the time point, all substrates presented significant differences with $p < 0.001$. $n = 3$; mean ± standard deviation is shown. (B) Live-dead images at the same magnification for specific time points, where live cells were labelled with green and the dead ones with red. The scale bar represents 200 μm.

that at an initial stage the release of silver is at higher concentrations and can penetrate the cell wall, entering into the cells and this way, can damage the DNA and reduce cell viability. The release of Ag was increasingly reduced after 72 hours; hence, we supposed that it could be an explanation for the great proliferation, indicated by the significant increase of metabolic activity, verified at day 7. As already said, when Ag nanoparticles were not present in the last layer, the release can take more time. It can compromise the cellular viability and metabolic activity, observed for the condition ending with CHT/HA; nonetheless, this decrease did not happen in the case of the coatings ending with CHT/HA–DN, which indicates that the DN effect overlaps the later Ag release effect. In our previous work,[11] we compared the cellular behavior of CHT/HA and CHT/HA–DN multilayers, using two types of cells: L929 and SaOs-2. We found that the catechol groups presented by DN-containing multilayers had a positive effect in terms of adhesion, proliferation, and viability compared with the multilayers without DN. Different authors[11,40,41] attributed the enhancement of the cellular behavior to the fact that the dopamine functional group can act as an active anchor between the material surface and the cells, allowing the formation of covalent and non-covalent bonds.

In addition, these results were reinforced by the fluorescence results of L929 adhered on the surface of each coating, at 1, 3 and 7 days, presented in Fig. S2 (ESI†). The cells were fixed and stained with two distinct fluorochromes, where the nuclei of the cells were stained with blue (DAPI) and their cytoskeleton was stained with red (phalloidin). The presented representative images were concordant with those obtained through the previous cellular behavior tests. For the condition $[CHT/HA/CHT/AgBG]_5$ + [CHT/HA], the rate of proliferation was slightest compared to that for the other conditions. Curiously, after 3 days, the cells seemed to stretch and gain the typical morphology of L929 cells and this was even more perceptible at day 7.

For the $[CHT/HA–DN/CHT/AgBG]_5$ + [CHT/HA–DN] condition, at day 3 the cells already present the characteristic morphology and at day 7 it was possible to observe a kind of fibroblastic network, where with the intense proliferative activity the cells adhered and occupied almost every space of the coating. The phenotype and morphology of the adhered cells for the conditions $[CHT/HA/CHT/AgBG]_5$ and $[CHT/HA–DN/CHT/AgBG]_5$ were similar; this could be related to the presence of AgBG nanoparticles, which were not uniformly distributed, as confirmed by AFM analysis included in the ESI† (Fig. S3), and this surface heterogeneity could induce the presence of a higher number of cells in a certain area.

Conclusions

This study emphasized that it was possible to successfully prepare LbL thin films which combine HA–DN, CHT and AgBG. The adhesive strength of the antibacterial thin films containing

HA–DN was significantly higher than that of the control film. *In vitro* bioactivity tests demonstrated the bioactive potential of these films induced by the presence of the produced silver nanoparticles. The microbiological assays showed that the addition of AgBG onto the films inhibited the bacterial growth after 16 h. In particular, it was interesting to note that films with the CHT/HA–DN end layer presented better adhesive strength and also enhanced cell adhesion, proliferation and viability.

From these results, it was found that these films could be potentially used as adhesive coatings for orthopedic implants in order to promote the formation of hydroxyapatite around the implant, improve both cell response and adhesion strength and also prevent the typical bacterial infections in a simple and versatile way. Further work is in progress testing these LbL configurations in the development of freestanding membranes that should be used for orthopedic applications.

Acknowledgements

The authors acknowledge the Portuguese Foundation for Science and Technology (FCT) and the European program FEDER/COMPETE for the financial support through project BioSeaGlue: EXPL/CTM-BIO/0646/2013 (FCOMP-01-0124-FEDER-041105). This work was co-funded by "Programa Operacional Regional do Norte" (ON.2-O Novo Norte) under the "Quadro de Referência Estratégico Nacional" (QREN), through the "Fundo Europeu de Desenvolvimento Regional" (FEDER). E. T. also thanks the FCT investigator grant (IF/01390/2014).

Notes and references

1 A. M. El-Kady, A. F. Ali, R. A. Rizk and M. M. Ahmed, *Ceram. Interfaces*, 2012, **38**, 177–188.
2 J. L. Dalsin, B. H. Hu, B. P. Lee and P. B. Messersmith, *J. Am. Chem. Soc.*, 2003, **125**, 4253–4258.
3 M. Yu, J. Hwang and T. J. Deming, *J. Am. Chem. Soc.*, 1999, **121**, 5825–5826.
4 M. J. Sever, J. T. Weisser, J. Monahan, S. Srinivasan and J. J. Wilker, *Angew. Chem., Int. Ed. Engl.*, 2004, **43**, 448–450.
5 H. Lee, Y. Lee, A. R. Statz, J. Rho, T. G. Park and P. B. Messersmith, *Adv. Mater.*, 2008, **20**, 1619–1623.
6 Y. Lee, H. Lee, Y. B. Kim, J. Kim, T. Hyeon, H. Park, P. B. Messersmith and T. G. Park, *Adv. Mater.*, 2008, **20**, 4154–4157.
7 M. Guvendiren, P. B. Messersmith and K. R. Shull, *Biomacromolecules*, 2008, **9**, 122–128.
8 A. Charlot, V. Sciannamea, S. Lenoir, E. Faure, R. Jerome, C. Jerome, C. Van De Weerdt, J. Martial, C. Archambeau, N. Willet, A.-S. Duwez, C.-A. Fustin and C. Detrembleur, *J. Mater. Chem.*, 2009, **19**, 4117–4125.
9 S. H. Ku, J. Ryu, S. K. Hong, H. Lee and C. B. Park, *Biomaterials*, 2010, **31**, 2535–2541.
10 S. C. Nicklisch and J. H. Waite, *Biofouling*, 2012, **28**, 865–877.
11 A. I. Neto, A. C. Cibrao, C. R. Correia, R. R. Carvalho, G. M. Luz, G. G. Ferrer, G. Botelho, C. Picart, N. M. Alves and J. F. Mano, *Small*, 2014, **10**, 2459–2469.
12 R. R. Costa and J. F. Mano, *Chem. Soc. Rev.*, 2014, **43**, 3453–3479.
13 M. Rinaudo, M. Milas and P. Le Dung, *Int. J. Biol. Macromol.*, 1993, **15**, 281–285.
14 R. Jayakumar, M. Prabaharan, R. L. Reis and J. F. Mano, *Carbohydr. Polym.*, 2005, **62**, 142–158.
15 G. Crini and P.-M. Badot, *Prog. Polym. Sci.*, 2008, **33**, 399–447.
16 N. M. Alves, I. B. Leonor, H. S. Azevedo, R. L. Reis and J. F. Mano, *J. Mater. Chem.*, 2010, **20**, 2911–2921.
17 S. Govindan, E. A. K. Nivethaa, R. Saravanan, V. Narayanan and A. Stephen, *Appl. Nanosci.*, 2012, **2**, 299–303.
18 J. R. Fraser, T. C. Laurent and U. B. Laurent, *J. Intern. Med.*, 1997, **242**, 27–33.
19 X. Zhang, Z. Li, X. Yuan, Z. Cui and X. Yang, *Appl. Surf. Sci.*, 2013, **284**, 732–737.
20 M. Bellantone, N. J. Coleman and L. L. Hench, *J. Biomed. Mater. Res.*, 2000, **51**, 484–490.
21 A. G. Gristina, *Science*, 1987, **237**, 1588–1595.
22 A. D. Russel, in *Disinfection, sterilization, and preservation*, ed. S. S. Block, Lippincott Williams & Wilkins, Philadelphia, 5th edn, 2001, ch. 3, pp. 31–55.
23 B. S. Liu and T. B. Huang, *Macromol. Biosci.*, 2008, **8**, 932–941.
24 M. Catauro, M. G. Raucci, F. De Gaetano and A. Marotta, *J. Mater. Sci.: Mater. Med.*, 2004, **15**, 831–837.
25 A. Balamurugan, G. Balossier, D. Laurent-Maquin, S. Pina, A. H. Rebelo, J. Faure and J. M. Ferreira, *Dent. Mater.*, 2008, **24**, 1343–1351.
26 M. V. Voinova, M. Rodahl, M. Jonson and B. Kasemo, *Phys. Scr.*, 1999, **59**, 391.
27 T. Kokubo and H. Takadama, *Biomaterials*, 2006, **27**, 2907–2915.
28 F. Hook, B. Kasemo, T. Nylander, C. Fant, K. Sott and H. Elwing, *Anal. Chem.*, 2001, **73**, 5796–5804.
29 S. J. Rego, A. C. Vale, G. M. Luz, J. F. Mano and N. M. Alves, *Langmuir*, 2016, **32**, 560–568.
30 I. Perelshtein, G. Applerot, N. Perkas, G. Guibert, S. Mikhailov and A. Gedanken, *J. Nanotechnol.*, 2008, **19**, 245705.
31 G. M. Luz and J. F. Mano, *J. Nanotechnol.*, 2011, **22**, 494014.
32 D. S. Couto, N. M. Alves and J. F. Mano, *J. Nanosci. Nanotechnol.*, 2009, **9**, 1741–1748.
33 X. Chatzistavrou, J. C. Fenno, D. Faulk, S. Badylak, T. Kasuga, A. R. Boccaccini and P. Papagerakis, *Acta Biomater.*, 2014, **10**, 3723–3732.
34 S. A. Brennan, C. Ni Fhoghlu, B. M. Devitt, F. J. O'Mahony, D. Brabazon and A. Walsh, *Bone Joint J.*, 2015, **97–b**, 582–589.
35 E. Moran, S. Masters, A. R. Berendt, P. McLardy-Smith, I. Byren and B. L. Atkins, *J. Infect.*, 2007, **55**, 1–7.
36 S.-B. Lee, C. González-Cabezas, K.-M. Kim, K.-N. Kim and K. Kuroda, *Biomacromolecules*, 2015, **16**, 2265–2275.
37 J. Wang, Z. Li, Y. Liang, S. Zhu, Z. Cui, H. Bao, Y. Liu and X. Yang, *Mater. Express*, 2015, **5**, 191–200.
38 F. Sambale, S. Wagner, F. Stahl, R. R. Khaydarov, T. Scheper and D. Bahnemann, *J. Nanomater.*, 2015, **2015**, 9.
39 P. Zhang, Z. Zhang and W. Li, *J. Nanomater.*, 2013, **2013**, 8.
40 H. Lee, S. M. Dellatore, W. M. Miller and P. B. Messersmith, *Science*, 2007, **318**, 426–430.
41 H. Lee, N. F. Scherer and P. B. Messersmith, *Proc. Natl. Acad. Sci. U. S. A.*, 2006, **103**, 12999–13003.